

NAVAL POSTGRADUATE SCHOOL MONTEREY, CALIFORNIA



THESIS

NUMERICAL SIMULATION OF THE FLOW FIELD ABOUT A MULTI-ELEMENT AIRFOIL WITH OSCILLATING FLAP

by

Miguel A. Ortiz
March, 1996

Thesis Advisor:
Co-Advisor:

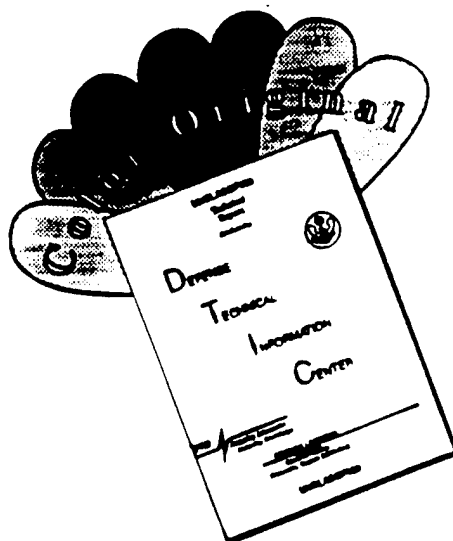
Max F. Platzer
Ismail H. Tuncer

Approved for public release; distribution is unlimited.

19960729 108

DTIC QUALITY INSPECTED 3

DISCLAIMER NOTICE



THIS DOCUMENT IS BEST QUALITY AVAILABLE. THE COPY FURNISHED TO DTIC CONTAINED A SIGNIFICANT NUMBER OF COLOR PAGES WHICH DO NOT REPRODUCE LEGIBLY ON BLACK AND WHITE MICROFICHE.

REPORT DOCUMENTATION PAGE

Form Approved OMB No. 0704-0188

Public reporting burden for this collection of information is estimated to average 1 hour per response, including the time for reviewing instruction, searching existing data sources, gathering and maintaining the data needed, and completing and reviewing the collection of information. Send comments regarding this burden estimate or any other aspect of this collection of information, including suggestions for reducing this burden, to Washington Headquarters Services, Directorate for Information Operations and Reports, 1215 Jefferson Davis Highway, Suite 1204, Arlington, VA 22202-4302, and to the Office of Management and Budget, Paperwork Reduction Project (0704-0188) Washington DC 20503.

1. AGENCY USE ONLY (Leave blank)	2. REPORT DATE March 1996.	3. REPORT TYPE AND DATES COVERED Master's Thesis	
4. TITLE AND SUBTITLE : NUMERICAL SIMULATION OF THE FLOW FIELD ABOUT A MULTI-ELEMENT AIRFOIL WITH OSCILLATING FLAP		5. FUNDING NUMBERS	
6. AUTHOR(S) Miguel A. Ortiz			
7. PERFORMING ORGANIZATION NAME(S) AND ADDRESS(ES) Naval Postgraduate School Monterey CA 93943-5000		8. PERFORMING ORGANIZATION REPORT NUMBER	
9. SPONSORING/MONITORING AGENCY NAME(S) AND ADDRESS(ES)		10. SPONSORING/MONITORING AGENCY REPORT NUMBER	
11. SUPPLEMENTARY NOTES The views expressed in this thesis are those of the author and do not reflect the official policy or position of the Department of Defense or the U.S. Government.			
12a. DISTRIBUTION/AVAILABILITY STATEMENT Approved for public release; distribution is unlimited.		12b. DISTRIBUTION CODE	
13. ABSTRACT (maximum 200 words) Investigation of steady and unsteady flowfields over airfoils is an active area of current computational and experimental research. In this study, the compressible, viscous, flow over a single and multi-element airfoil is numerically simulated by solving the Navier Stokes equations. The motivation for this work includes interest in studying the effects of a stationary/flapping airfoil combination in tandem configuration. A single-block Navier- Stokes (NS) solver is employed to compute unsteady flowfields. Turbulence is treated using the Baldwin-Lomax turbulence model. A single C-grid is generated and it is partially distorted to simulate the flapping motion. Numerical solutions are obtained for flows at a fixed angle of attack and for unsteady flows over flapping airfoils. The numerical solutions agree well with the experimental data. The difficulties faced during the study are discussed and future improvements are suggested.			
14. SUBJECT TERMS *CFD, Unsteady Flow, Oscillating Airfoil, Grid Generation.		15. NUMBER OF PAGES 52	
		16. PRICE CODE	
17. SECURITY CLASSIFICATION OF REPORT Unclassified	18. SECURITY CLASSIFICATION OF THIS PAGE Unclassified	19. SECURITY CLASSIFICATION OF ABSTRACT Unclassified	20. LIMITATION OF ABSTRACT UL

NSN 7540-01-280-5500

Standard Form 298 (Rev. 2-89)
Prescribed by ANSI Std. Z39-18 298-102

DTIC QUALITY INSPECTED 3

Approved for public release; distribution is unlimited.

NUMERICAL SIMULATION OF THE FLOW FIELD ABOUT A MULTI-ELEMENT AIRFOIL WITH OSCILLATING FLAP

Miguel A. Ortiz
Lieutenant Commander, United States Navy
B.S., Embry-Riddle Aeronautical University, 1982

Submitted in partial fulfillment
of the requirements for the degree of


MASTER OF SCIENCE IN AERONAUTICAL ENGINEERING

from the


NAVAL POSTGRADUATE SCHOOL


March 1996

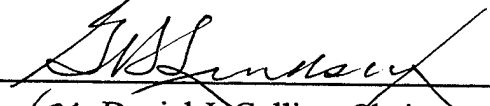
Author:


Miguel A. Ortiz

Approved by:


Max F. Platzer, Thesis Advisor


Ismail H. Tuncer, Co-Advisor


for Daniel J. Collins, Chairman
Department of Aeronautics and Astronautics

ABSTRACT

Investigation of steady and unsteady flowfields over airfoils is an active area of current computational and experimental research. In this study, the compressible, viscous flow over a single and multi-element airfoil is numerically simulated by solving the Navier Stokes equations. The motivation for this work includes interest in studying the effects of a stationary/flapping airfoil combination in tandem configuration. A single-block Navier- Stokes (NS) solver is employed to compute unsteady flowfields. Turbulence is treated using the Baldwin-Lomax turbulence model. A single C-grid is generated and it is partially distorted to simulate the flapping motion. Numerical solutions are obtained for flows at a fixed angle of attack and for unsteady flows over flapping airfoils. The numerical solutions agree well with the experimental data. The difficulties faced during the study are discussed and future improvements are suggested.

TABLE OF CONTENTS

I. INTRODUCTION	1
II. METHOD	3
A. GRID GENERATION	3
1. <i>Code Validation Grid</i>	3
2. <i>Unsteady Case I and II Grids</i>	6
B. ALGORITHM.....	7
1. <i>Navier-Stokes Solver</i>	7
2. <i>Boundary Conditions</i>	9
3. <i>Unsteady-Motion Routine</i>	9
III. RESULTS AND DISCUSSION.....	11
A. CODE VALIDATION	11
1. <i>Conditions--Steady State</i>	11
B. UNSTEADY CASE	14
1. <i>Case I</i>	14
2. <i>Case II</i>	22
IV. CONCLUSIONS AND RECOMMENDATIONS.....	23
A. CONCLUSIONS.....	23
B. RECOMMENDATIONS.....	23
LIST OF REFERENCES.....	25
APPENDIX A.....	27
A. DESCRIPTION OF NS INPUT FILE PARAMETERS	27
B. STEADY-STATE CONDITIONS.....	29
C. UNSTEADY CONDITIONS	29
D. GRMOVE (MOTION SUBROUTINE)	29
APPENDIX B	33
A. GRIDGEN INPUT FILE (NACA 4412).....	33
B. ELLIPTICAL SOLVER PROCESS	35
INITIAL DISTRIBUTION LIST	37

LIST OF FIGURES

FIGURE 1	PROPULSIVE FORCE ON PLUNGING AIRFOIL. NEACE [REF. 2]	1
FIGURE 2	EXPERIMENTAL CONFIGURATION ADAIR AND HORNE [REF.5].....	3
FIGURE 3	INITIAL CONFIGURATION GRID	4
FIGURE 4	CRITICAL WAKE AREA	5
FIGURE 5	AFT-FLAP WIND TUNNEL GRID.....	6
FIGURE 6	CASE I (TOP) AND II GRIDS(BOTTOM)	7
FIGURE 7	TRANSITION FUNCTION- HYPERBOLIC TANGENT	10
FIGURE 8	CONVERGENCE HISTORY INITIAL CONFIGURATION	11
FIGURE 9	AERODYNAMIC LOADS - INITIAL CONFIGURATION.....	12
FIGURE 10	COMPUTED VS. EXPERIMENTAL CP DISTRIBUTION.....	12
FIGURE 11	COMPUTED FLOWFIELD - INITIAL CONFIGURATION (TOP), AFT-FLAP AT $\delta_f=13.6^\circ$ (BOTTOM)	13
FIGURE 12	MASS-FLUX STEADY-STATE (TOP) AND UNSTEADY (BOT)	15
FIGURE 13	VELOCITY MAGNITUDE COMPUTED FOR STEADY-STATE (TOP) AND UNSTEADY (BOTTOM), $A=0.10c$, $K=.5$	16
FIGURE 14	MAIN AIRFOIL CP DISTRIBUTION $A=0.10c$, $K=.5$	17
FIGURE 15	BOUNDARY LAYER PROFILE, STEADY STATE (TOP), UNSTEADY (BOTTOM), $A = 0.10c$, $K = .5$	17
FIGURE 16	VELOCITY MAGNITUDE COMPUTED FOR STEADY-STATE (TOP) AND UNSTEADY (BOTTOM), $A=0.05c$, $K=.5$	18
FIGURE 17	TIME HISTORY OF THE UNSTEADY LIFT AND DRAG COEFFICIENTS	19
FIGURE 18	PARTICLE TRACES, LOWER POSITION (TOP), CENTER POSITION (BOTTOM)	20
FIGURE 19	PARTICLE TRACES , TRAVELING UP THROUGH WAKE (TOP), UPPER POSITION (BOTTOM)	21
FIGURE 20	VELOCITY MAGNITUDE COMPUTED FOR STEADY-STATE (TOP), $K = .5$ (CENTER) AND $K=1.0$ (BOTTOM).....	22

LIST OF SYMBOLS

c	model chord length
C_L	Lift coefficient
C_D	Drag coefficient
M	Mach number
L	Lift force
A	Plunging amplitude
α	angle-of-attack
δ_f	Flap deflection angle
ω	Frequency of oscillation
k	Reduced frequency
U_∞	Freestream velocity
h	Flap location
NS	Navier Stokes solver
LE	Leading edge
TE	Trailing edge

ACKNOWLEDGEMENTS

I would like to give my sincere appreciation to professor M. F. Platzer, my thesis advisor, for his guidance, and encouragement that kept me going throughout the completion of this research.

I would also like to thank professor I. H. Tuncer, my thesis co-advisor, for his guidance, technical assistance through his gifted knowledge of CFD, the NPS computer systems, and many hours of council that led to the successful completion of this work.

Finally, I would like to thank my lovely wife, Waleska, and my girls, Mileska, Ivette, Jeanette, and Jasmine, for their encouragement, support, and patience during my time at Naval Postgraduate School.

I. INTRODUCTION

Studies of steady and unsteady flowfields over multi-element airfoils is an active area of numerical and experimental research. While notable progress is being made in the development of computing methods to analyze flows around single airfoils, methods to compute more complex geometric configurations are now being developed. In this study, a Navier Stokes solver was modified to accommodate the complexity of a multi-element configuration to study the thrust generating effect of a stationary /flapping airfoil combination.

Thrust generation due to airfoil flapping was recognized by early researchers, such as Knoller [Ref. 1], in explaining the bird's ability to generate a propulsive force by means of flapping their wing. Previous experimental investigations of unsteady flows over oscillating airfoils by Neace [Ref. 2], Tuncer and Platzer [Ref. 3], and Dohring [Ref. 4] have shown a propulsive effect and the associated efficiencies. Figure 1 shows how the airfoil motion creates an induced velocity component. This allows for the generation of a forward or thrust component of force.

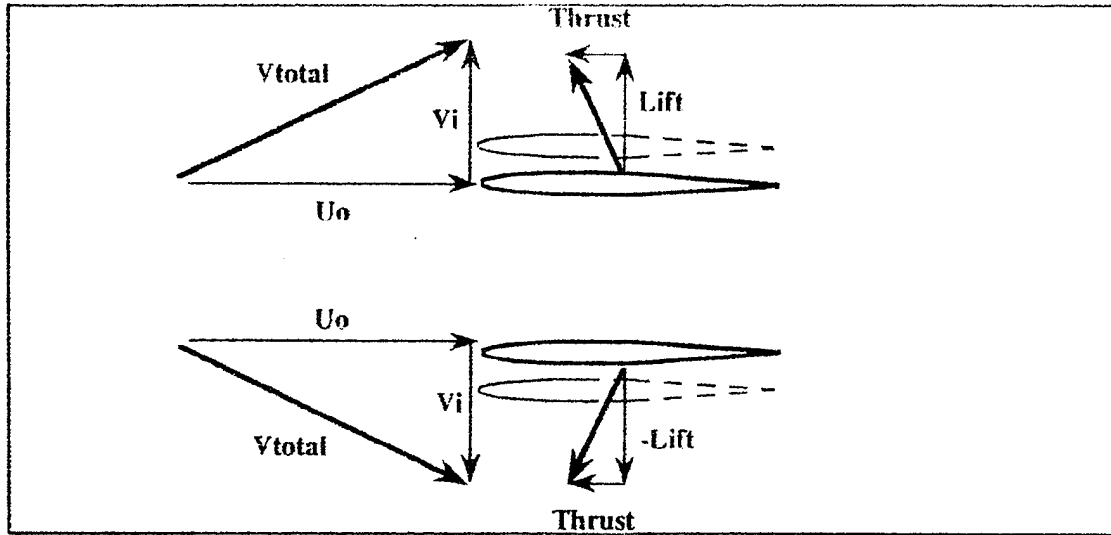


Figure 1 Propulsive Force on Plunging Airfoil. Neace [Ref. 2]

In the process of this research, a single block Navier Stokes solver was first validated on a Ames-01 airfoil. The solver was subsequently modified to handle multi-element airfoil configurations utilizing a single structured C-grid. Computational grids

were generated utilizing GRIDGEN . Other grid generating tools were evaluated, but only GRIDGEN provided the flexibility to properly distribute the gridlines in critical areas. The initial grid configuration utilizing NACA 4412 and 4415 airfoils within a wind tunnel boundary was used in the validation process of the code. Two other configurations were studied under unsteady conditions . In the unsteady flow case the leading airfoil is kept stationary while the trailing airfoil undergoes a flapping motion. In Case I, flap is placed at .5c aft of the main airfoil and in Case II at .25c aft of the main airfoil These two cases were studied at different flapping frequencies and amplitudes.

II. METHOD

A. GRID GENERATION

1. Code Validation Grid

During the grid generation process proper distribution of grid points around the airfoil's leading edge and trailing edge, orthogonality of the grid lines on the surface, and smooth variations of the grid density are the most critical factors. In order to accurately calculate the flow gradients in the direction normal to the surface in the boundary layer, it is necessary to make the normal grid spacing very fine close to the solid surfaces. Single C-type grids for NACA 4412 (Main airfoil) and NACA 4415 (Flap) were generated for the code validation process modeling the configuration in Figure 2. The grids included in this report were generated using GRIDGEN software packages.

Adair and Horne [Ref. 5] conducted experiments with this configuration in the 7 by 10 Foot Wind Tunnel at NASA Ames Research Center. In the experiment, the chord length of the main airfoil is .90 m and that of the flap is .36 m. The geometric location of the flap relative to the main airfoil was described by the flap gap (FG), the flap overlap (FO) and the flap deflection (δ_f). For this case $FG = 0.035c$, $FO = 0.028c$, $\delta_f = 21.8^\circ$ and the main airfoil angle of attack (α) was set to 8.2° .

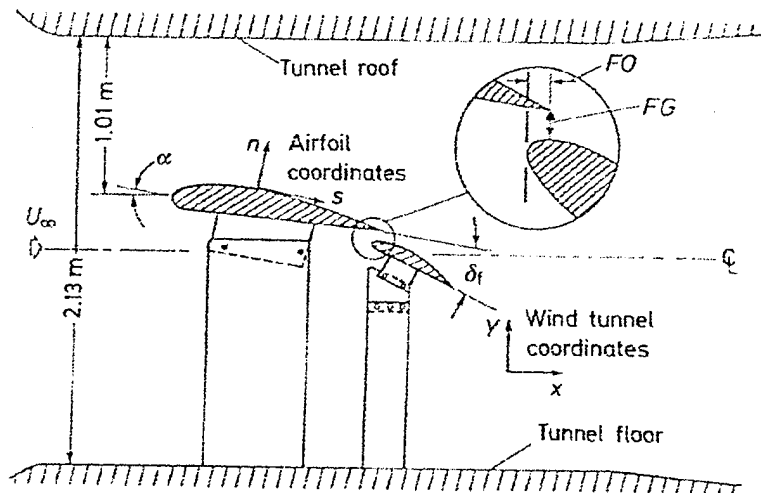


Figure 2 Experimental Configuration Adair and Horne [Ref.5]

The proximity of the airfoils, and the sensitivity of the solver puts a heavy constraint on the computational grid around the downstream airfoil. In this case it was not possible to duplicate the exact positioning of the flap. Instead, the flap was positioned at $0.015c$ aft of the main airfoil, as shown in Figure 3, and a parametric study on the flap overlap and gap was conducted to verify proper trends and extrapolate verification. To improve the resolution and distribution of the gridlines in the wake of

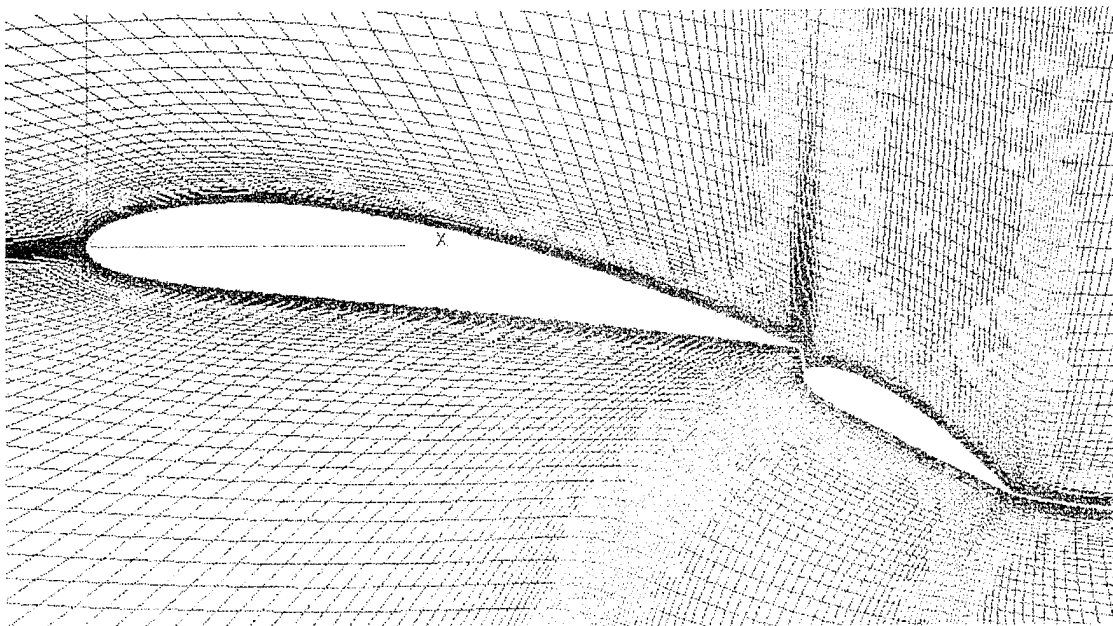


Figure 3 Initial Configuration Grid

the main airfoil GRIDGEN's elliptical solver was used. One of the main reasons for using an elliptic solver is to force the grid to have a smooth variation while maintaining the grid as body fitted. The other reason is the ability of the solution to provide clustering and orthogonality to the grid based on the control function selected. GRIDGEN offers a choice of four control function types that influences the grid distribution and orthogonality. Among those, the Laplace control function with a .7 relaxation parameter was the standard selection for this research. This type of function is the least computationally demanding and the most stable. This method produces the smoothest possible grid. For a detailed description of all related parameters see the GRIDGEN Manual [Ref. 6]. See sample of GRIDGEN input file and elliptical solver parameters in the Appendix B.

The following is a list of parameters and procedures used to run the elliptical solver:

- Relaxation factor = 0.7
- Laplace control function
- Set BC's on the airfoil surface to orthogonality. By default all points on the edges will remain fixed as the elliptical solver is run.
- Turn foreground BC's on (elliptical solver menu) with default values.
- Run the solver for critical areas separately, this will expedite the process and will result in a smoother grid.
- Run the solver until an acceptable grid is achieved.

Figure 4 shows the grid distribution in the wake area for the initial configuration and the up-flap configuration. For the aft-flap configuration the flap was moved aft 0.03c, for the up-flap configuration the flap was moved up from the aft position 0.03c. Due to the positioning of the flap in the wake of the main airfoil, (up-flap configuration) the density of the grid lines between airfoils was increased. The grid dimensions for the initial and up-flap configurations were 361 x 100 and 463 x 100, respectively.

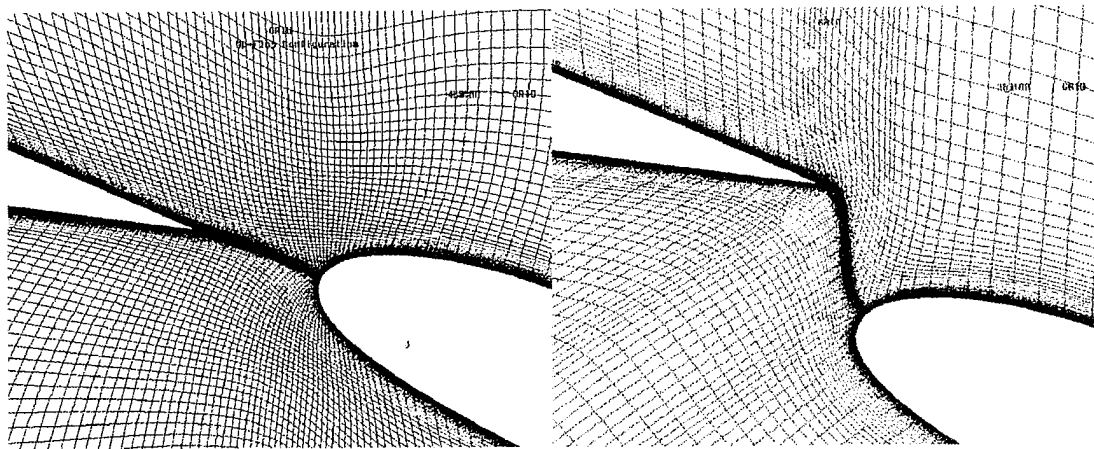


Figure 4 Critical Wake Area

Figure 5 shows the full wind tunnel model for the aft-flap configuration used during the validation process.

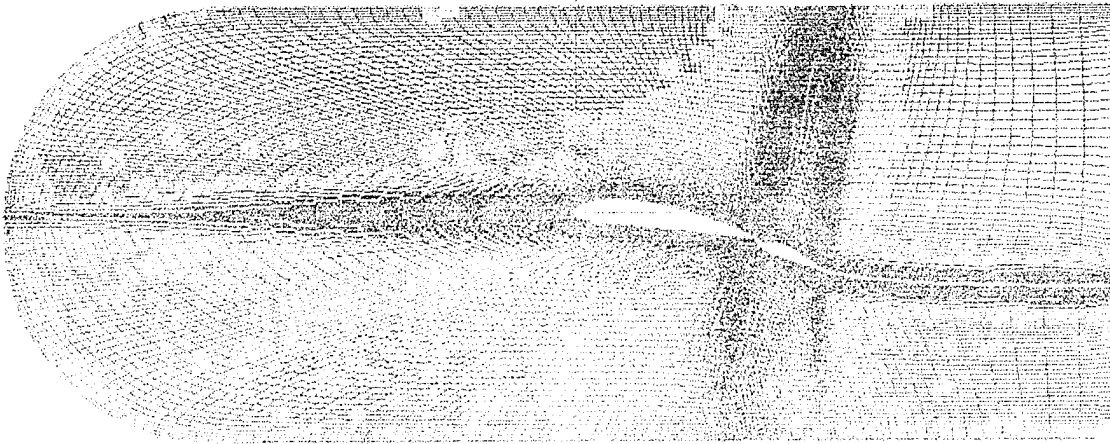


Figure 5 Aft-flap Wind Tunnel Grid

2. Unsteady Case I and II Grids

For unsteady computations two separate grids were generated as Case I and II. NACA 4412 and 4415 airfoils were used for these computations. The airfoil combination was set in a tandem configuration with a gap between airfoils of $.5c$ for Case I and $.25c$ for Case II. (Figure 6). The length of the flap (NACA 4415) was set to $0.33c$. The main airfoil was set at $\alpha = 10^\circ$ and the flap at zero angle of attack with respect to the main airfoil chord line. The grid dimensions are 391×100 for Case I and 371×100 for Case II.

These configurations eliminate some of the complexities of the initial configuration grid allowing the evaluation of the oscillation effects without the influence of any other variables. In addition, having the trailing airfoil far enough from the main airfoil facilitates the implementation of distortion required to model the oscillation process. Details of the grid distortion are discussed in the next section.

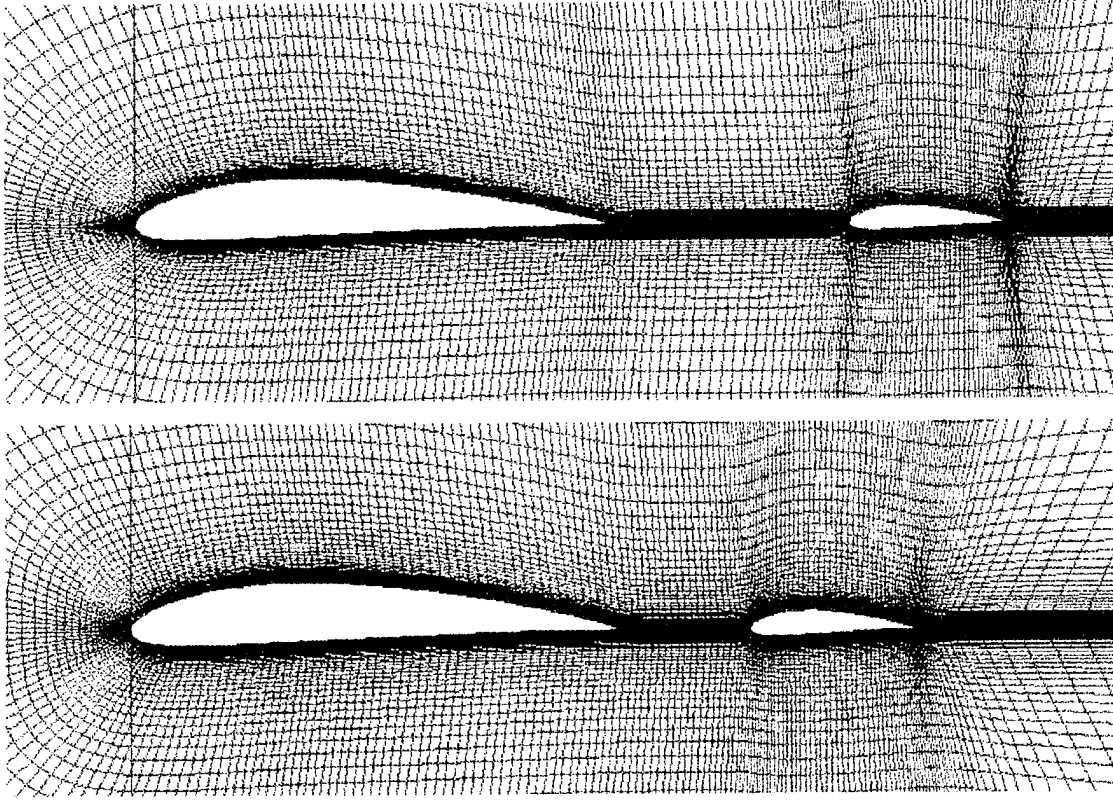


Figure 6 Case I (top) and II grids(bottom)

B. ALGORITHM

1. Navier-Stokes Solver

An implicit, thin layer, Navier-Stokes solver with the third order accurate Osher's upwind biased flux difference splitting scheme is employed to compute the flowfield in the computational grid. The strong conservation law form of the 2-D, thin layer Navier-Stokes equations in a curvilinear coordinate system, (ξ, ζ) , along the axial and normal direction respectively, is given as follows

$$\partial_t \hat{Q} + \partial_\xi \hat{F} + \partial_\zeta \hat{G} = (\text{Re})^{-1} \partial_\zeta \hat{S} \quad (2.1)$$

Where \hat{Q} is the vector of conservative variables, $1/J(\rho, \rho u, \rho w, e)$, \hat{F} and \hat{G} are the inviscid flux vectors, and \hat{S} is the thin layer approximation of the viscous fluxes in the ζ direction normal to the airfoil surface:

$$\hat{F} = \frac{1}{J} \begin{pmatrix} \rho U \\ \rho u U + \xi_x p \\ \rho w U + \xi_z p \\ (e + p)U - \xi_t p \end{pmatrix}, \quad \hat{G} = \frac{1}{J} \begin{pmatrix} \rho W \\ \rho u W + \zeta_x p \\ \rho w W + \zeta_z p \\ (e + p)W - \zeta_t p \end{pmatrix}$$

$$\hat{S} = \frac{1}{J} \begin{pmatrix} 0 \\ \mu m_1 u_\zeta + (\mu/3)m_2 \zeta_x \\ \mu m_1 w_\zeta + (\mu/3)m_2 \zeta_z \\ \mu m_1 m_3 + (\mu/3)m_2 + (\zeta_x u + \zeta_z w) \end{pmatrix} \quad (2.2)$$

where

$$m_1 = \zeta_x^2 + \zeta_z^2 \quad (2.3)$$

$$m_2 = \zeta_x u_\zeta + \zeta_z w_\zeta$$

$$m_3 = (u^2 + w^2) / 2 + \kappa \text{Pr}^{-1} \left(\frac{\partial^2}{\partial \zeta} \right)$$

and U, W are the contravariant velocity components. In the above equations, all dimensions are normalized with the airfoil chord length, c . ρ is the density normalized with the free-stream density ρ_∞ ; u and w are the Cartesian velocity components in the physical domain, which are normalized with the free-stream speed of sound a_∞ ; e is the total energy per unit volume normalized with $\rho_\infty a_\infty^2$; and Pr is the Prandtl number. The pressure is related to density and total energy through the equation of state for an ideal gas, $p = (\gamma - 1)[e - \rho(u^2 + w^2) / 2]$. (2.4)

The flowfield is assumed to be fully turbulent. The turbulence modeling is used to relate the Reynolds shear stress to the local mean-velocity gradient allowing numerical flow field calculation. The Baldwin--Lomax algebraic turbulence model is currently implemented. This model is a two layer eddy viscosity model which simulates the effect of turbulence in terms of eddy viscosity coefficient. A complete description of the model is given in Baldwin [Ref. 7].

2. Boundary Conditions

The computational domain includes both airfoil surfaces and extends ten chord lengths away from the airfoils. Boundary conditions are applied on the airfoil surfaces, and at the farfield boundaries. On the airfoil surfaces the no slip boundary condition is applied. For the flapping airfoil, the surface fluid velocity is set equal to the prescribed airfoil flapping velocity so that the no slip condition is satisfied. Since the formulation of the Navier-Stokes solver is based on an inertial frame of reference, the flapping motion of the airfoil is implemented by moving the airfoil and the computational grid around it in the transverse direction as described by the frequency and the amplitude of the flapping motion by:

$$h = -A \cos(\omega t) \quad (2.5)$$

Where A denotes the mean amplitude normalized with the chord length. ω is the frequency of the oscillatory flapping motion, which is used in terms of reduced frequency,

$$k = \omega c / 2U_{\infty} \quad (2.6)$$

At the farfield inflow and outflow boundaries the flow variables are evaluated using the zero order Riemann invariant extrapolation.

For the code validation studies, no slip boundary condition is applied at the tunnel walls.

3. Unsteady-Motion Routine

The features pertinent to the grid distortion in the NS code were modified so that the trailing airfoil can move in the cross-flow direction with respect to the leading airfoil. During the flapping motion the main airfoil remains stationary while the flap oscillates in the cross flow direction. This motion is introduced by a partial grid distortion. The wake region between airfoils is the area of concern since the distortion is gradually introduced from the trailing edge of the main airfoil to the flap leading edge. During this distortion the integrity of the grid in terms of orthogonality, smoothness and clustering of grid point should remain physically valid for a solution to converge. In order to maintain a smooth variation of grid distortion a hyperbolic tangent is used as the transition function between

the stationary and moving part of the grid.. The grid's distortion adjusts smoothly using this function. Figure 7 shows this function. The grid motion routine (GRMOVE subroutine of the NS code) is given in the Appendix A.

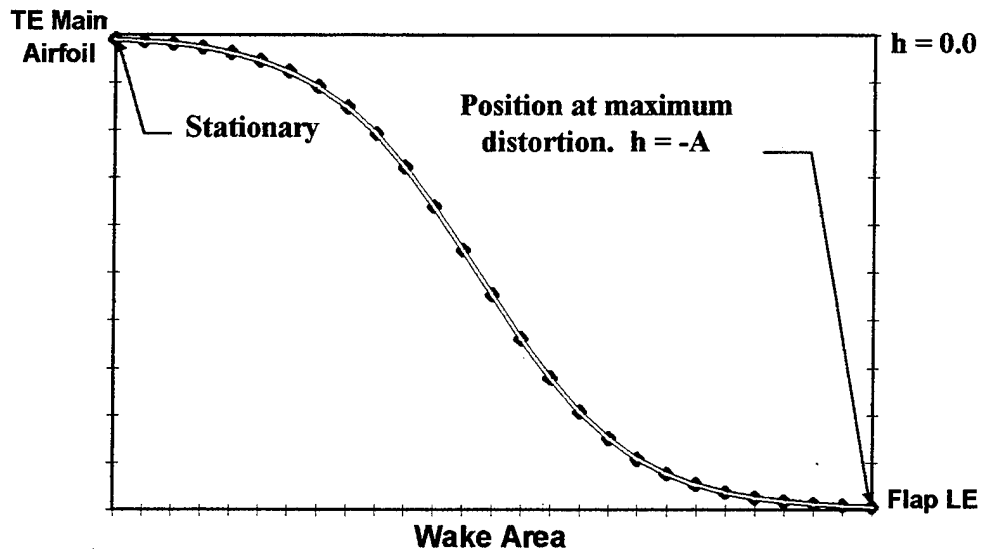


Figure 7 Transition Function- Hyperbolic Tangent

III. RESULTS AND DISCUSSION

The validity of the code was first tested with a specified configuration. The code was tested under the steady-state conditions described below. The solution was then evaluated for a number of configurations and compared to the experimental data. Following the validation process the flowfield with the flapping trailing airfoil was studied for two different configurations.

A. CODE VALIDATION

1. Conditions--Steady State

For the validation process the flowfield was computed at:

- $\alpha = 8.2^\circ$
- Mach = .2
- Reynolds number 1.8×10^6 , fully turbulent.

The solver was first run with the initial wing-flap configuration. Convergence was reached at 1500 iterations based on the variations in the flow residuals and the aerodynamic loads. Similarly, the solver was run for the aft-flap and up-aft flap configurations. A typical NS input file is shown in the Appendix A. Figure 8 shows the convergence history of the initial case and Figure 9 shows the aerodynamic loads for the same configuration.

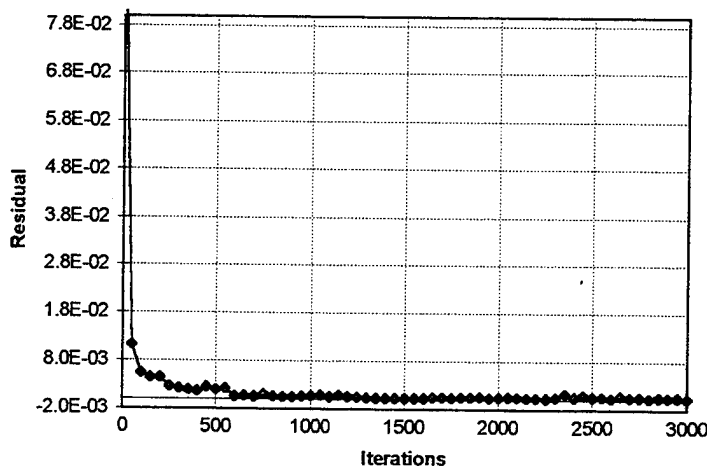


Figure 8 Convergence History Initial Configuration

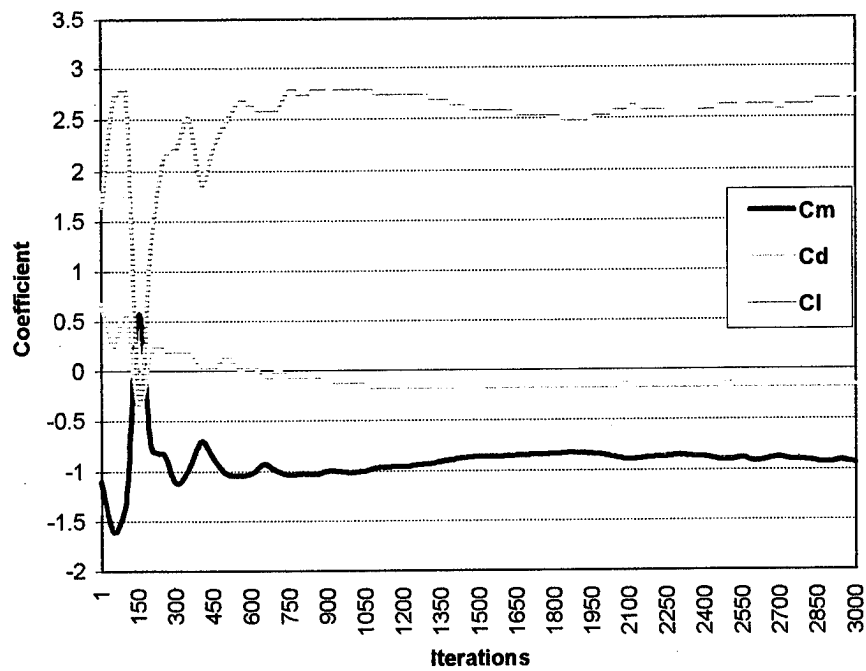


Figure 9 Aerodynamic Loads - Initial Configuration

Figure 10 shows the pressure coefficient distribution for all cases. The pressure changes indicated in this figure for the different cases shows a general trend that represents a

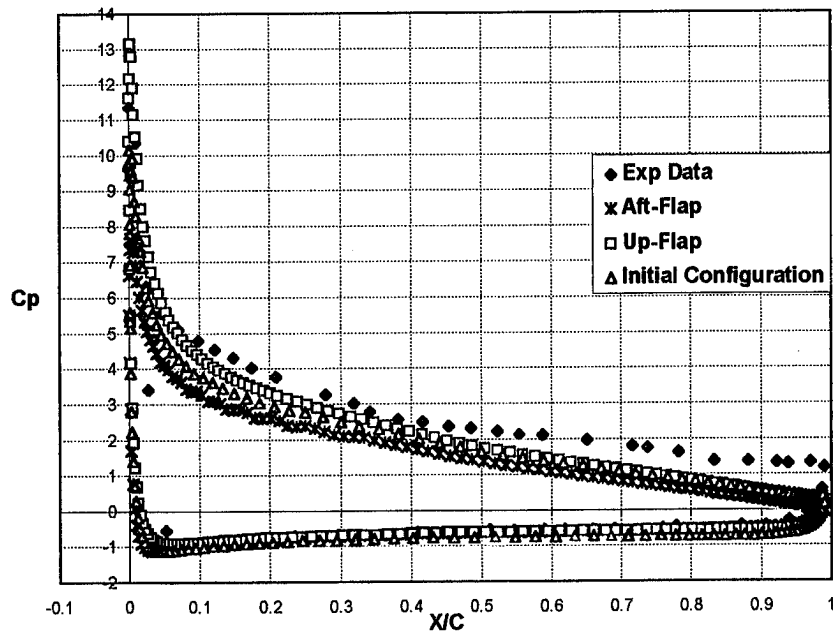


Figure 10 Computed vs. Experimental C_p Distribution

good agreement with the experimental data. Figure 11 summarizes the effects of the gap on the separated flap flow. This figure shows how the flowfield is affected as the flap is lowered or moved aft. As the gap is increased more fluid from below the main airfoil moves into the flap through the gap pushing the flow farther away from the flap leading edge, Alemdaroglu [Ref. 8]. As the gap is increased the flow will move the streamlines upward affecting the flow separation over the flap. This condition has significant effect on the pressure distribution over the aft-upper surface of the main airfoil as noted in Figure 10.

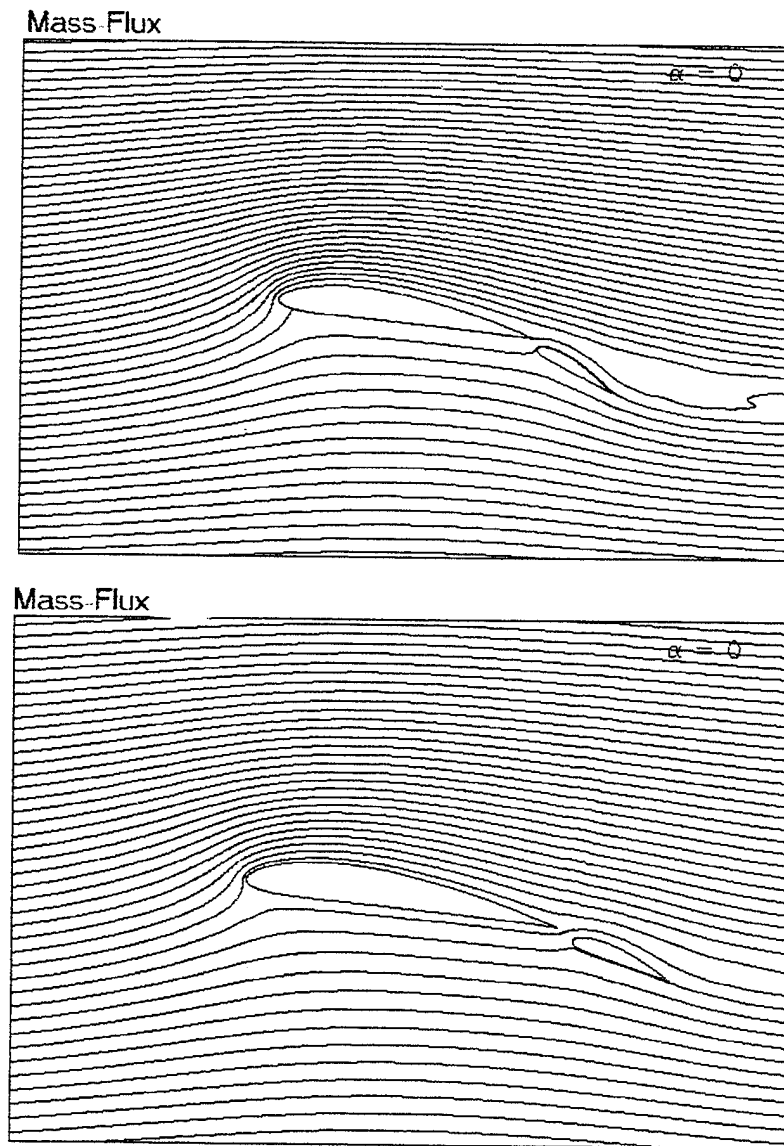


Figure 11 Computed flowfield - Initial Configuration (top), Aft-flap at $\delta_f = 13.6^\circ$ (bottom)

B. UNSTEADY CASE

This part of the research focused on the aerodynamic interaction between two NACA airfoils as shown in Figure 6. The main airfoil (NACA 4412) is stationary while the flap (NACA 4415) undergoes a flapping motion. The flowfields were evaluated under the following conditions:

- $\alpha = 10$ degrees
- Mach = .3
- Reynolds number 3.93×10^6

The unsteady computations were initialized with a steady-state solution computed at the maximum flapping amplitude where the flapping velocity is zero, Tuncer and Platzer [Ref. 3]. See a copy of the input file in the Appendix A. The unsteady computations were carried out for up to three periods of harmonic flapping motion. The flowfields presented were taken from the last period of the computation cycle. All unsteady runs were completed at the Naval Postgraduate School Cray Y-MP J94. The average computer processing time (CPU) for 15,000 time step of unsteady computations was 9.21 hours.

1. Case I

The flowfield for this case was initially computed with a flapping motion of $A = .10c$ and $k = 0.5$. The computed streamlines for both the steady and unsteady case are shown in Figure 12. It can be noted in this figure that the fluid particles no longer travel freely through the gap to the upper flap section. Instead, the suction created by the flapping motion keeps the dividing streamline closer to the flap leading edge. The flow fields for both the steady-state and unsteady solution are shown in Figure 13.

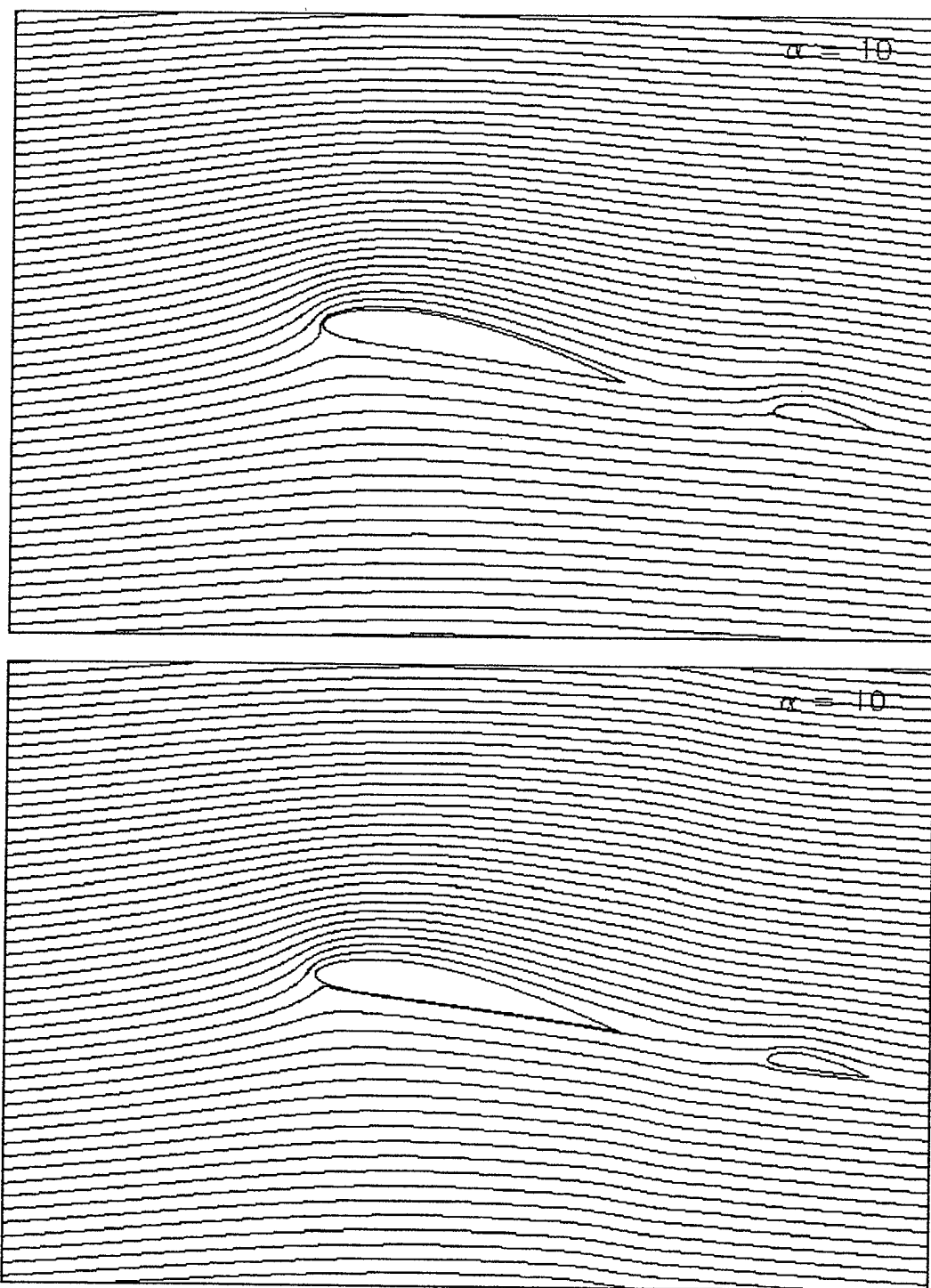


Figure 12 Mass-Flux Steady-State (top) and Unsteady (bot)

Figure 13 clearly shows that the flow is sucked toward the flap if the flap is oscillating.

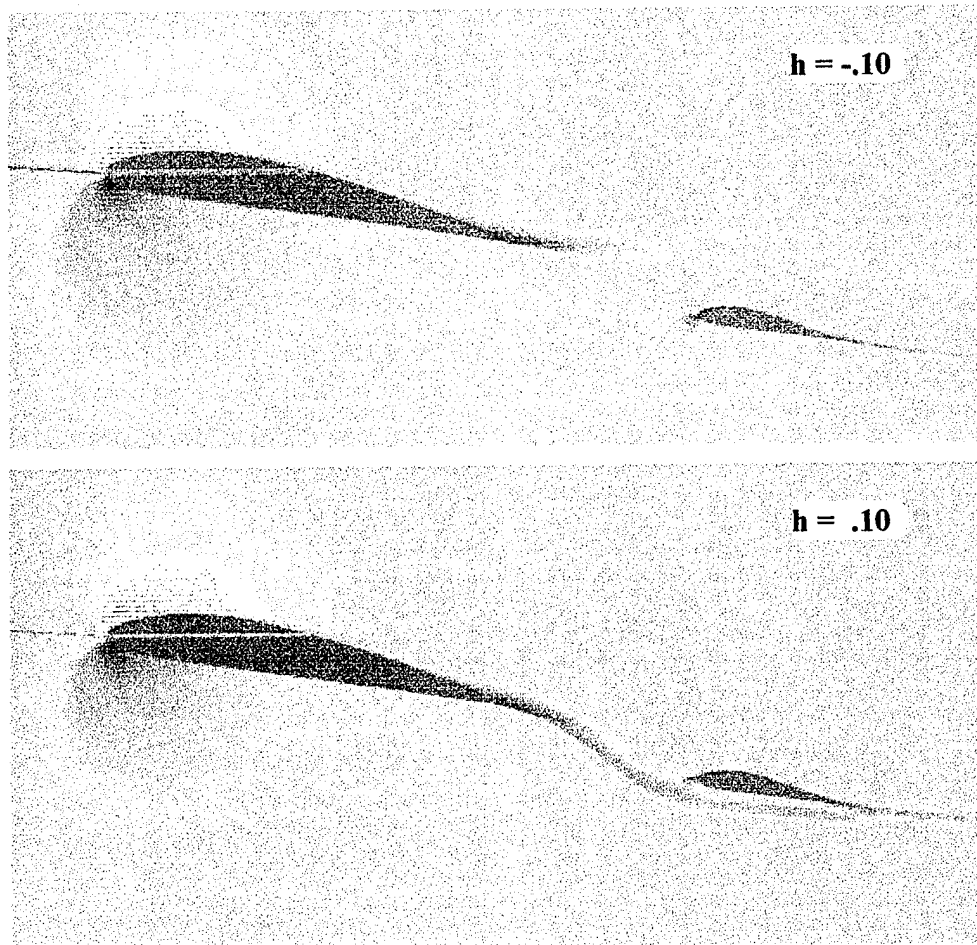


Figure 13 Velocity Magnitude Computed for Steady-State (top) and Unsteady (bottom),
 $A=0.10c$, $k=.5$

Due to the gap size the effect on pressure distribution over the main airfoil was very small as shown in Figure 14. On the other hand, the boundary layer profile changes, shown in Figure 15, at the aft upper surface of the main airfoil are significant. It is noted that the flow reversal is reduced, the magnitude of the velocity vectors is increased and the boundary layer reattaches to the surface close to the trailing edge. The changes are really noticeable in the trailing edge region which indicates that the suction produced by the flapping airfoil is not sufficient for a reattachment of the boundary layer forward of that region.

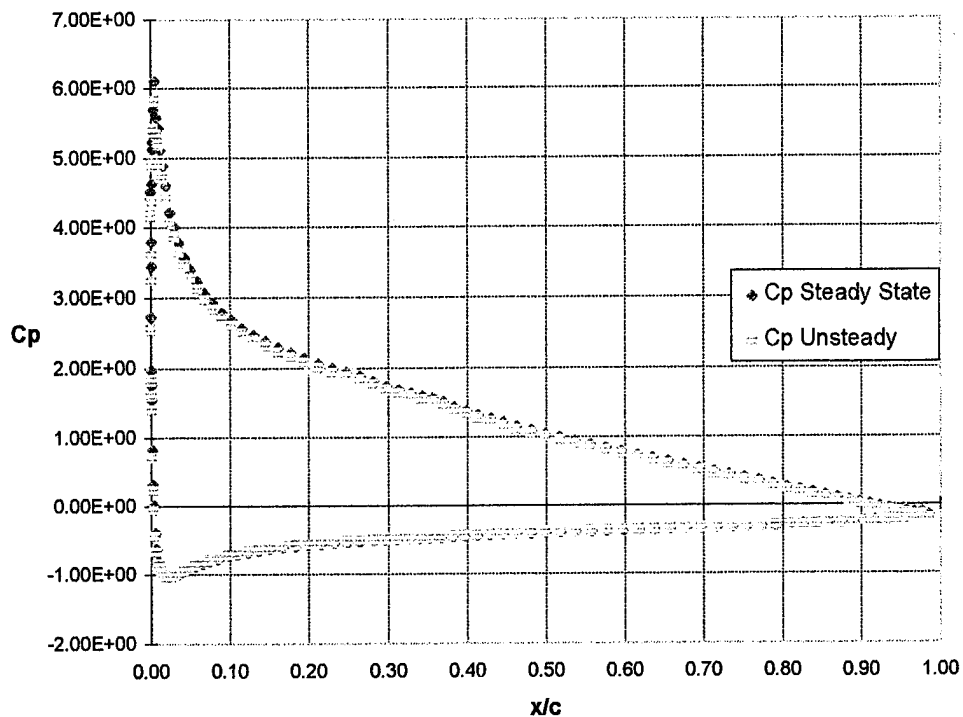


Figure 14 Main Airfoil Cp Distribution $A=0.10c$, $k=.5$

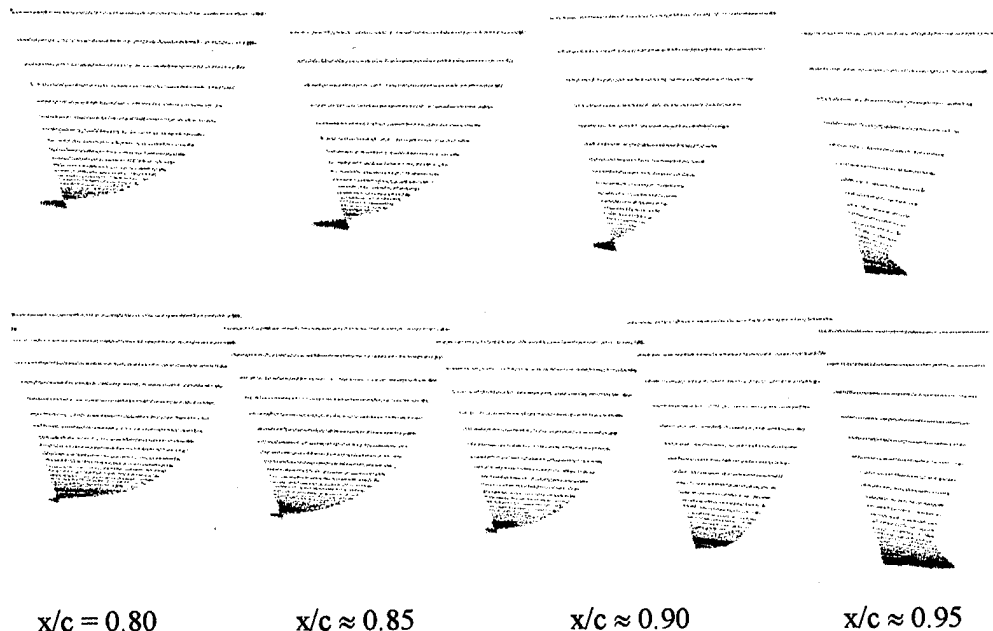
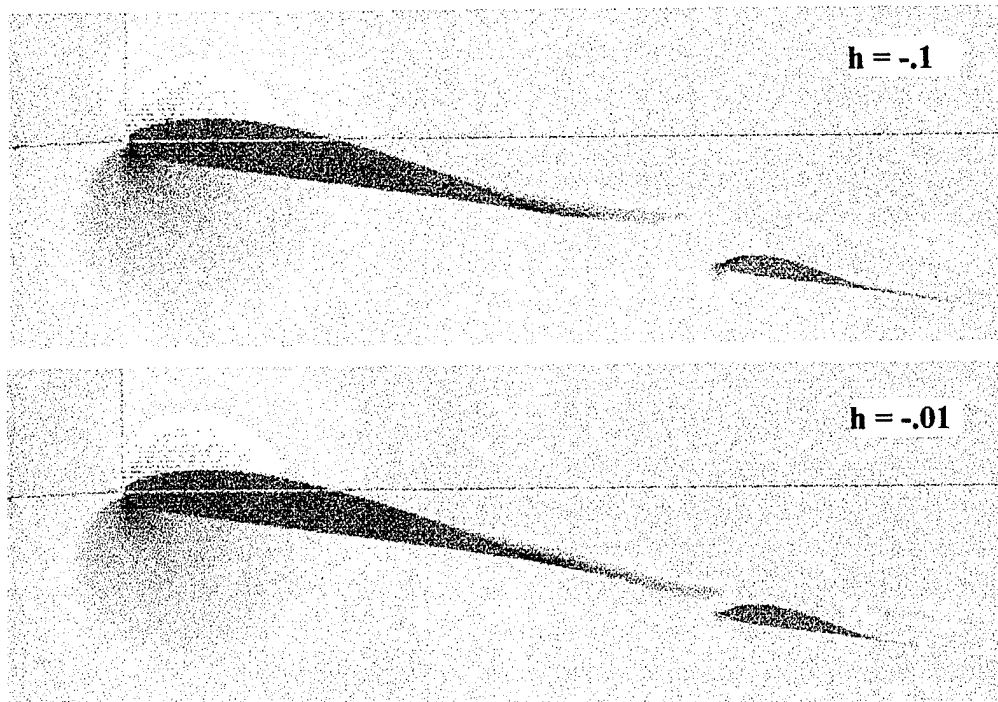


Figure 15 Boundary Layer Profile, Steady State (top), Unsteady (bottom), $A = 0.10c$, $k = .5$

The case I configuration was tested at $A = 0.05$ and $k = .5$, with very similar results, as shown in Figure 16. This figure suggests that due to the reduced oscillating amplitude the suction effect was significantly reduced.



*Figure 16 Velocity Magnitude Computed for Steady-State (top) and Unsteady (bottom),
 $A=0.05c$, $k=.5$*

The time history of the unsteady aerodynamic loads of the flapping motion is shown in Figure 17. Following the initial transition, all aerodynamic loads attain a periodic behavior with respect to the flapping motion. For the lift coefficient the oscillation created peak variations of less than one percent for both cases. Similarly, drag coefficient variations were less than 2.5 percent for $A=.1c$ and one percent for $A=.05c$.

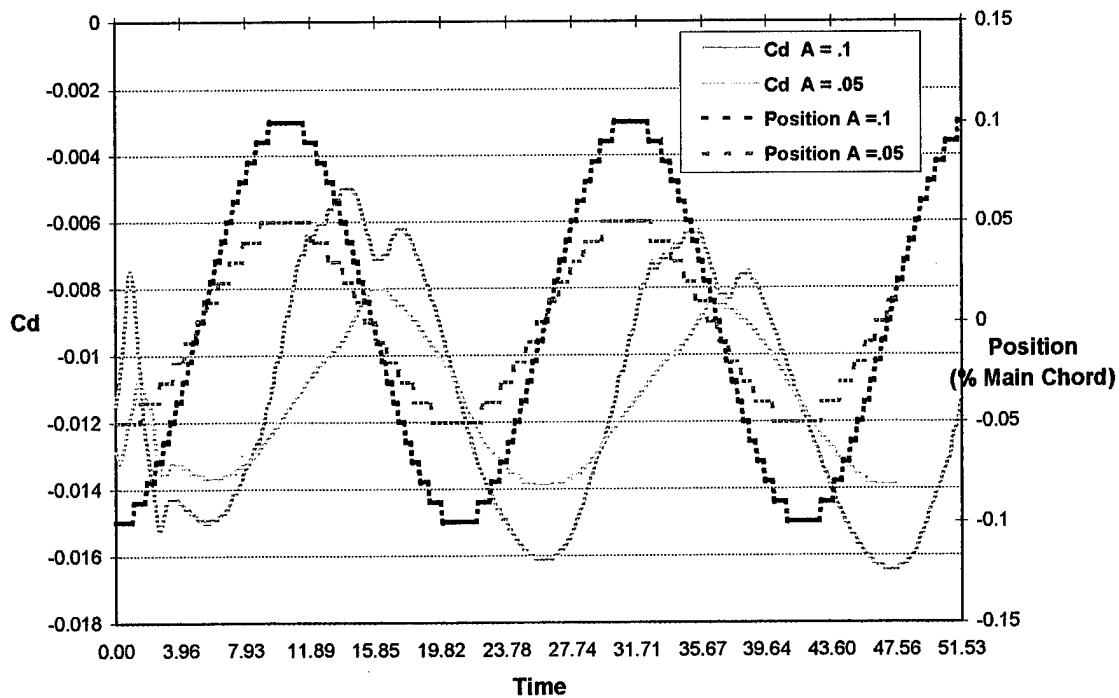
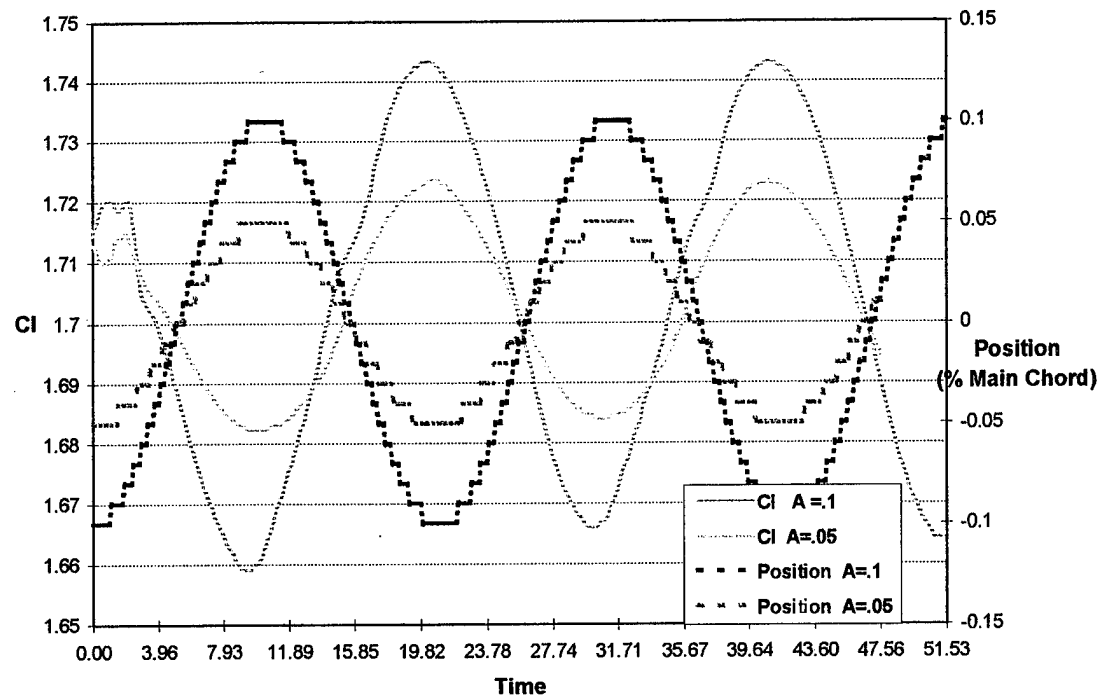


Figure 17 Time History of the Unsteady Lift and Drag Coefficients

Figures 18 and 19 shows the particle traces for four different flap positions.

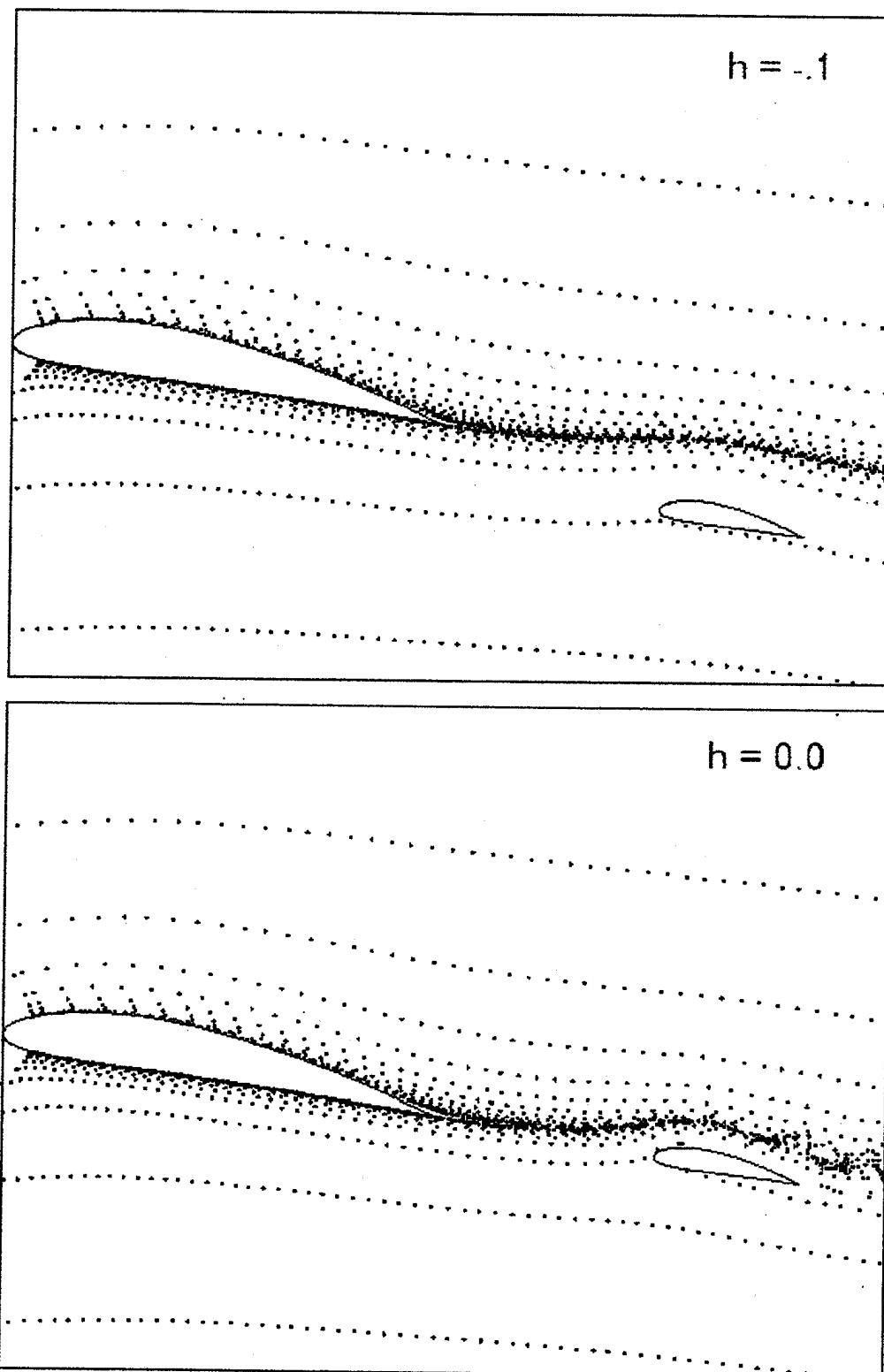


Figure 18 Particle Traces, Lower Position (top), Center Position (bottom)

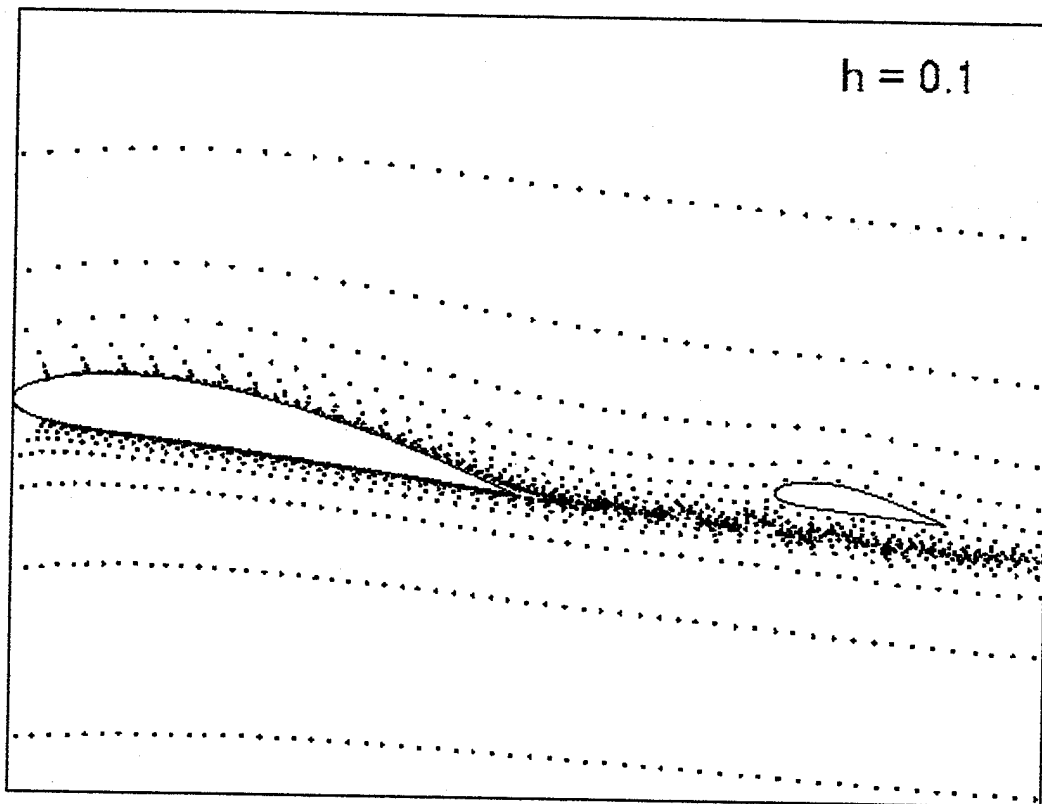
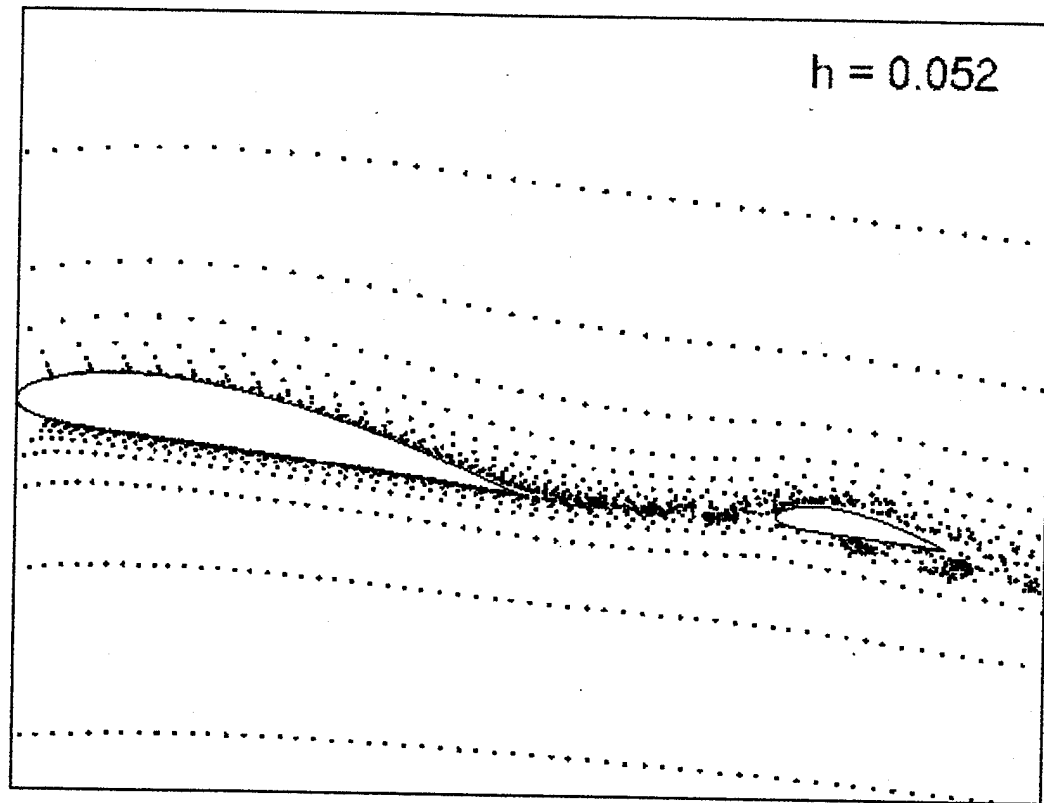


Figure 19 Particle Traces , Traveling Up through Wake (top), Upper Position (bottom)

2. Case II

For this case the gap between airfoils was changed to $.25c$. Solutions were obtained for $A = .05$ and $k = .5$ and 1.0 . Figure 20 shows how changes in oscillating frequency influence the thrust generation. As frequency increases, the suction increases pulling the wake of the main airfoil closer to the flap boundary.

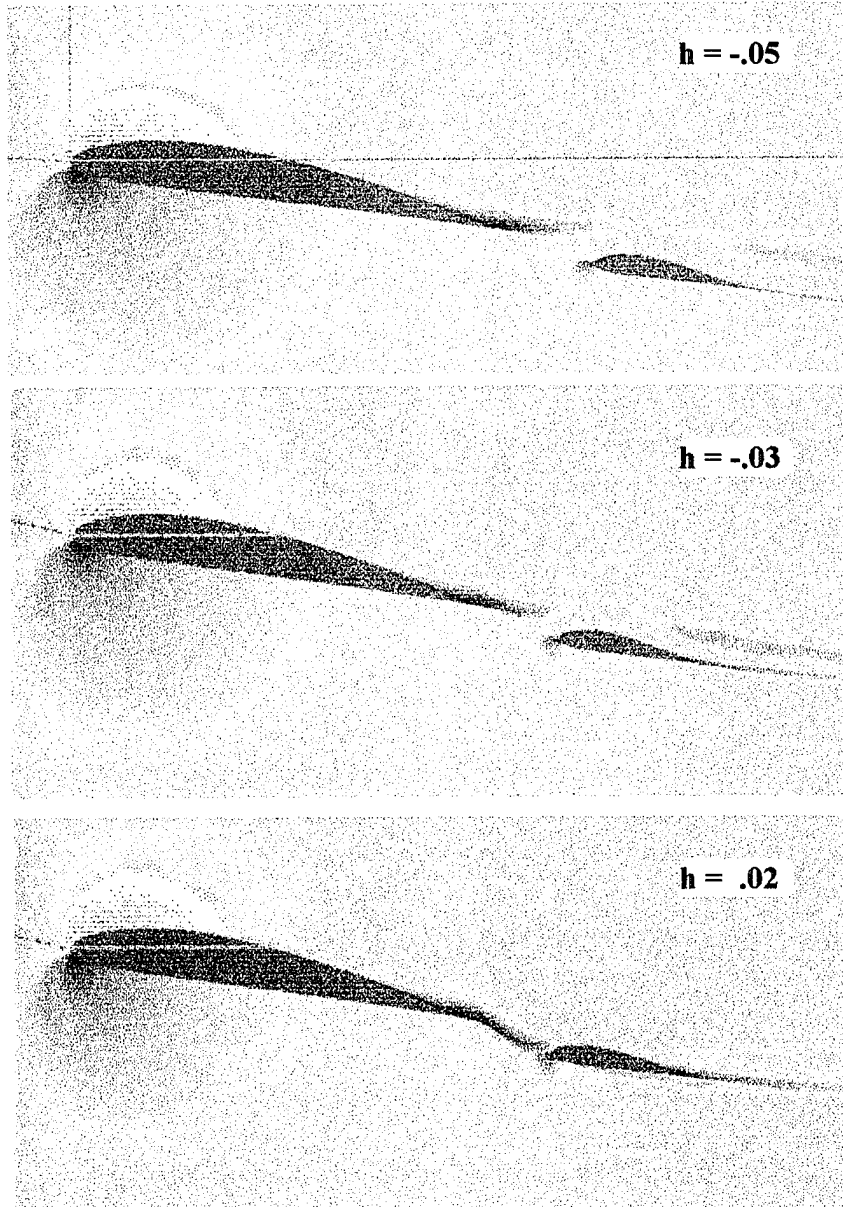


Figure 20 Velocity Magnitude Computed for Steady-State (top), $k = .5$ (center) and $k=1.0$ (bottom)

IV. CONCLUSIONS AND RECOMMENDATIONS

A. CONCLUSIONS

Subsonic flow over stationary airfoil/oscillating flap combinations were computed using a Navier-Stokes solver. The computed flowfields confirm the observations made in recent experiments performed by Dohring [Ref. 4]. However additional computations for other configurations at different frequencies, amplitudes, angle-of-attack, airfoil sections, etc., are required before more quantitative conclusion can be drawn. Preliminary review of the computed boundary layer characteristics indicates that with a proper configuration and applying a proper combination of the flapping parameters mentioned above a reattachment of the boundary layer may result.

B. RECOMMENDATIONS

To fully satisfy the goals of this research a wider parametric study is required. In order to obtain a clear picture of the flapping effects and to be able to quantify the thrust efficiency the effect of the following parameters listed below needs to be identified.

- Frequency of oscillation
- Amplitude
- Reynolds number
- Gap size and flap location
- Angle-of-attack
- Airfoil section (i.e. symmetric, non-symmetric, flat plate, etc.)

In addition;

1. The complexity of the flow, especially in the wake area of both airfoils, requires special attention. For complex turbulent flows, the choice of turbulence model will have a significant impact on accuracy and computational time. Therefore, other turbulence model, such as k- ϵ or Baldwin-Barth, needs to be investigated for the multi-element configuration, Nelson [Ref. 9].

2. Grid generation is critical toward obtaining accurate solutions. Tools currently available are complex. Therefore, more work is required to create a grid that solves the overhang and overlap problem discussed in the grid generation section. A multi-block grid may solve this problem.

LIST OF REFERENCES

1. Knoller, R., "Die Gesetze des Luftwiderstandes, " Flug-und Motortechnik, Vol. 3, No.21, 1909, pp.1-7.
2. Neace, K., "A Computational and Experimental Investigation of the Propulsive and Lifting Characteristics of Oscillating Airfoils and Airfoil Combinations in Incompressible Flow," Master's Thesis, Naval Postgraduate School, Monterey, California, Sep 1992.
3. Tuncer, I. H., and Platzler, M. F., "Thrust Generation Due To Airfoil Flapping," AIAA Journal, Vol. 34, No. 2, pp. 324-331, Feb 1996.
4. Dohring, C., "Thrust Due to Airfoil Flapping and it's Applications to Boundary Layer Control," Ph.D. Thesis in preparation, Naval Postgraduate School, Monterey, California.
5. Adair, D., and Horne, W.C., "Turbulent Separated Flow Over and Downstream of a Two-element Airfoil," Experiments in Fluids, Vol. 7, No. 8, 1989.
6. Laboratory Manual for The Gridgen 3D Multiple Block Grid Generator System, General Dynamics Corporation, Vol. 2, Feb 1991.
7. Baldwin, B. S., Lomax, H., "Thin Layer Approximation and Algebraic Model For Separated Turbulent Flows, " AIAA Paper 78-257, Jan 1978.
8. Alemdaroglu, N., "Experimental Investigation of the Flow Around a Multielement Airfoil," Advisory Group for Aerospace Research & Development, Conference Proceedings 515, Sep 1993.
9. Nelson, T. E., "Compressible Navier-Stokes Computations of Multielement Airfoil Flows Using Multiblock Grids," AIAA Journal, Vol. 32, No. 3, Mar 1994.

APPENDIX A

A. DESCRIPTION OF NS INPUT FILE PARAMETERS

IREAD	0	No initial solution, free stream conditions initialize the flowfield in the startup steady-state computations
	1	Initial solution is read from a binary file saved from the previous run (default, at the end of each run, solution file is saved as binary)
	2	Initial solution is read as formatted (plot3d form)
	-1	Initial solution is read as binary, unsteady motion starts
	-2	Initial solution is read as formatted (plot3d form), unsteady motion starts
ITER -	# of timesteps	
NPRINT	Residuals are printed out at every nprint timesteps	
NLOAD	Aerodynamic loads are printed out at every nload timesteps	
ODVAR	Solution variables, q array, are written into "qp.d" file at every delta odvar change in unsteady motions (degrees in oscillatory motion, amplitude change in plunge)	
ALPHA	Steady state AOA (do not set it to zero, instead set it to 0.0001)	
OSCIL	false	N/A
	true	sinusoidal oscillations in pitch
RAMP	false	N/A
	true	straight ramp motion in pitch
REDFRE	Reduced frequency of the unsteady pitching motion based on the half chord, chord length is assumed to be 1.	
ALFAMND	Min AOA of the pitching motion	
ALFAMXD	Max AOA of the pitching motion	
PLUNGE	false	N/A
PLMX	Plunge amplitude in x	
PLMY	Plunge amplitude in y	

PLPHSXD	The Phase angle between x and y amplitudes, in degrees
PLFREQ	The reduced frequency of the plunging motion based on the half chord, chord length is assumed to be 1.
REYNOLD	Reynolds number of the freestream flowfield
MACH	Mach number of the freestream flowfield
VISC	false Euler solution true Viscous Navier-Stokes solution
TURBL	false Laminar flow is assumed. true Baldwin-Lomax turbulence model is applied.
TRANS	false Fully turbulent flow is assumed. true BL transition with Michel criterion is modeled. A steady-state solution has to be obtained first. TIMEACC has to be set to true.
TIMEACC	false Variable local time stepping in the computational grid, used in the computations of steady state and/or attached flowfields. true Constant time stepping everywhere in the computational grid, used in the computations of unsteady and separated flowfields
COUR	Courant number of the timestepping (50-1500), determines the timestep of the computations based on the minimum grid size and the freestream conditions. Its value depends on the computational grid. For diverging computations, when the residuals in the output file increases in time, it is the sign that its value is to be reduced.
NEWTIT	Number of Newton subiterations in each timestep, applied in unsteady flows (2-3), for steady flowfields it is set to 1.
POTEN	This variable is reserved for NS-Potential flow interactive solution procedure.

The NS program needs, in general, the following input files:

ns.in: Input file which defines certain parameters as given above. It is set up for starting a generic steady-state solution. For continuing computations or for any changes in the input variables you need to edit this file.

grid.in : A formatted file in which the computational grid coordinates are stored.

strs.d : A file in which the starting solution is stored. Could be binary or formatted in

accordance with the IREAD variable.

Once you have the input files ready, you can run the NS solver on SGI's by simply submitting it with the following command at the prompt:

```
run ns
```

B. STEADY-STATE CONDITIONS

```
C.. IREAD, NITER  NPRINT, NLOAD ODVAR
   0          3000   10      10      0.01
C.. ALPHA  OSCIL  RAMP  REDFRE  ALFAMND  ALFAMXD
   10.0      false   false  0.099   0.001   10.0
C.. PLUNGE  PLMX   PLMY  PLPHSXD  PLFREQ
   false     0.      0.10   0.      0.5
C.. MACH    REYNOLD  VISC  ITURBL  TRANS
   0.300    3930000. true    1      false
C.. TIMEACC  COUR  NEWTIT
   false     100.   1
```

C. UNSTEADY CONDITIONS

```
C.. IREAD, NITER  NPRINT, NLOAD ODVAR
  -2        13000   20      20      0.01
C.. ALPHA  OSCIL  RAMP  REDFRE  ALFAMND  ALFAMXD
   10.0      false   false  0.099   0.001   10.0
C.. PLUNGE  PLMX   PLMY  PLPHSXD  PLFREQ
   true      0.0     0.10   0.0     0.5
C.. MACH    REYNOLD  VISC  ITURBL  TRANS
   0.300    3930000. true    1      false
C.. TIMEACC  COUR  NEWTIT
   true      500.   1
```

D. GRMOVE (MOTION SUBROUTINE)

```
subroutine grmove(dalfa,dx,dz)
  include 'coms.f'
  dimension xold(nia,nka), zold(nia,nka)
  do i=1,imx(1)
  do k=1,kmx(1)
  xold(i,k) = x(i,k)
  zold(i,k) = z(i,k)
  enddo
```

```

enddo

if( dalfa .ne. 0.) then
    ca = cos( dalfa )
    sa =-sin( dalfa )
    do i=1,imx(1)
        do k=1,kmx(1)
            x(i,k) = xold(i,k) * ca - zold(i,k) * sa
            z(i,k) = zold(i,k) * ca + xold(i,k) * sa
        enddo
    enddo
endif
IF( dx .ne. 0. .or. dz .ne. 0. ) then
if(.not. distort) then
    do k=1,kmx(1)
        do i=1,imx(1)
            x(i,k) = x(i,k) + dx
            z(i,k) = z(i,k) + dz
        enddo
    enddo
else
    kinner = 45
    kouter = 80
    iinner1 =89
    iinner2 =283
    iouter1 =108
    iouter2 =264
    xrangeinner = 3.5
    xrangeouter = 2.
    yrangeinner = 2.
    yrangeouter = 2.
    do i=1,imx(1)
        if (i .le. iinner1 .and. i .ge. 1) then
            xfactor = 1
        elseif (i .ge. iinner2 .and. i .le. imx(1)) then
            xfactor = 1
        elseif (i .lt. iouter1 .and. i .gt. iinner1) then
            slope = -(yrangeinner+yrangeouter)/
> float((iouter1-1)-(iinner1+1))
            xcept = yrangeinner-slope*float(iinner1+1)
            yinput = slope*float(i)+xcept
            xfactor = 0.5*(tanh(yinput)+1.)
        elseif (i .gt. iouter2 .and. i .lt. iinner2) then
            slope = (yrangeinner+yrangeouter)/
> float((iinner2-1)-(iouter2+1))

```

```

xcept = xrangeinner-slope*float(iinner2+1)
yinput = slope*float(i+2)+xcept
xfactor = 0.5*(tanh(yinput)+1.)
else
    xfactor = 0.
endif

    do k=1,kmx(1)
        if( k .le. kinner ) then
            factor = 1.
        elseif( k .gt. kinner .and. k .lt. kouter ) then
            slope = -(xrangeinner+xrangeouter)/
> float((kouter-1)-(kinner+1))
            xcept = xrangeinner-slope*float(kinner+1)
            xinput = slope*float(k)+xcept
            factor = 0.5*(tanh(xinput)+1.)
        else
            factor = 0.
        endif
        xold(i,k) = x(i,k)
        zold(i,k) = z(i,k)
        x(i,k) = x(i,k) + dx
        z(i,k) = z(i,k) + dz*factor * xfactor
    enddo
    enddo
endif
ENDIF

if( unstdy ) then
    do k=1,kmx(1)
        do i=1,imx(1)
            xtau(i,k) = (x(i,k) - xold(i,k))/dtau
            ztau(i,k) = (z(i,k) - zold(i,k))/dtau
        enddo
    enddo
else
    do k=1,kmx(1)
        do i=1,imx(1)
            xtau(i,k) = 0.
            ztau(i,k) = 0.
        enddo
    enddo
endif

call metric

```

```

if( .not. unstdy .or. itr .eq. niter ) then
open(unit=91,file='grid.out',form='formatted')
write (91,*) imx(1), kmx(1), iwks(1), iwall
write (91,*) ((x(i,k), i = 1, imx(1)), k = 1,kmx(1) ),
>      ((z(i,k), i = 1, imx(1)), k = 1,kmx(1) )
endif

return
end

```

APPENDIX B

A. GRIDGEN INPUT FILE (NACA 4412)

100		
1.833333	0	0
1.832997	-1.4E-05	0
1.831988	-5.7E-05	0
1.830313	-0.00013	0
1.827978	-0.00023	0
1.824994	-0.00036	0
1.821375	-0.00051	0
1.817136	-0.0007	0
1.812297	-0.00091	0
1.806878	-0.00116	0
1.800905	-0.00143	0
1.794402	-0.00173	0
1.787397	-0.00206	0
1.779921	-0.00243	0
1.772005	-0.00282	0
1.763682	-0.00325	0
1.754987	-0.00371	0
1.745956	-0.00421	0
1.736626	-0.00473	0
1.727034	-0.00528	0
1.717219	-0.00586	0
1.707221	-0.00646	0
1.697078	-0.00708	0
1.68683	-0.00771	0
1.676518	-0.00834	0
1.66618	-0.00896	0
1.655855	-0.00956	0
1.645584	-0.01013	0
1.635403	-0.01066	0
1.625516	-0.01116	0
1.615838	-0.01167	0
1.60636	-0.01216	0
1.597109	-0.01264	0
1.588117	-0.01307	0
1.579412	-0.01343	0
1.571021	-0.01371	0
1.562971	-0.0139	0
1.55529	-0.01397	0
1.548004	-0.01391	0
1.541138	-0.01371	0
1.534718	-0.01336	0
1.528769	-0.01284	0
1.523314	-0.01216	0
1.518378	-0.0113	0
1.513983	-0.01025	0

1.510148	-0.00902	0
1.506894	-0.0076	0
1.504238	-0.00599	0
1.502195	-0.00419	0
1.500779	-0.00219	0
1.5	0	0
1.500433	0.00471	0
1.501666	0.007159	0
1.503578	0.009655	0
1.506166	0.012185	0
1.509425	0.014728	0
1.513346	0.017264	0
1.517917	0.019767	0
1.523122	0.022211	0
1.528943	0.02457	0
1.535358	0.026815	0
1.54234	0.028917	0
1.549861	0.030851	0
1.557887	0.032591	0
1.566384	0.034114	0
1.575313	0.035397	0
1.584631	0.036424	0
1.594297	0.03718	0
1.604266	0.037653	0
1.614489	0.037837	0
1.624921	0.037726	0
1.63547	0.037324	0
1.645972	0.036695	0
1.656548	0.035879	0
1.667154	0.034885	0
1.677746	0.033726	0
1.688281	0.032416	0
1.698716	0.03097	0
1.709009	0.029403	0
1.71912	0.027731	0
1.729007	0.025973	0
1.738634	0.024145	0
1.747962	0.022265	0
1.756955	0.020352	0
1.76558	0.018425	0
1.773803	0.016503	0
1.781595	0.014604	0
1.788926	0.012748	0
1.795769	0.010954	0
1.802101	0.009241	0
1.807898	0.007626	0
1.813139	0.006128	0
1.817806	0.004762	0
1.821884	0.003544	0
1.825358	0.002489	0
1.828216	0.001607	0

1.830449	0.00091	0
1.83205	0.000407	0
1.833012	0.000102	0
1.833333	0	0

B. ELLIPTICAL SOLVER PORCESS

- Select Domain commands from GRIDGEN's main menu.
 - ◆ Select the domain to be solved.
- Set solver attributes (Boundary conditions)
 - ◆ Foreground control function
 - ⇒ Enable surface edges (ON)
 - ⇒ Edge influence (ON)
 - ⇒ Enter ΔS delay factor = 10. (Number of gridlines from the surface for which these conditions apply.)
 - ⇒ Enter angle decay factor = 10. (Angle gridlines makes with the boundary itself.)
 - ◆ Background control function
 - ⇒ Select Laplace function
 - ◆ Done with settings
 - ◆ Run solver.

INITIAL DISTRIBUTION LIST

1. Defense Technical Information Center2
8725 John J. Kingman Rd. STE 0944
Ft. Belvoir, VA 22060-6218
2. Dudley Knox Library2
Naval Postgraduate School
4111 Dyer Rd.
Monterey, CA 93943-5101
3. Mr. Max F. Platzer
Department of Aeronautics and Astronautics, Code AA/PI10
Naval Postgraduate School
Monterey, CA 93943-5101
4. Mr. Ismail H. Tuncer
Department of Aeronautics and Astronautics, Code AA/Tu1
Naval Postgraduate School
Monterey, CA 93943-5101
5. LCDR Miguel A. Ortiz2
105 Shubrick Road
Monterey, CA 93940